

ARTICLE

<https://doi.org/10.1038/s41467-019-09509-y>

OPEN

A chloroplast structured photocatalyst enabled by microwave synthesis

Shuning Xiao¹, Dieqing Zhang¹, Donglai Pan¹, Wei Zhu¹, Peijue Liu¹, Yong Cai¹, Guisheng Li¹ & Hexing Li¹

Photosynthesis occurs through the synergistic effects of the non-continuously distributed components in the chloroplast. Inspired by nature, we mimic chloroplast and develop a generic approach to synthesize non-continuously distributed semiconductors threaded by carbon nanotubes. In the synthesis, carbon nanotubes serve as microwave antennas to produce local super-hot dots on the surface, which might induce and accelerate various organic/inorganic semiconductors assembly. With the unique nanoscale designed bionic architecture, a chloroplast structured photocatalyst with 3-dimensional dual electron transfer pathways facilitate enhanced photocatalytic performance. The as-synthesized carbon nanotubes-titanium oxide achieves a record-breaking efficiency of 86% for nitric oxide treatment under ultraviolet light irradiation. As a general strategy, a wide variety of carbon nanotubes threaded chloroplast structured nanomaterials can be synthesized and these nanomaterials could find applications in energy chemistry, environmental science and human health.

¹Key Laboratory of Resource Chemistry of Ministry of Education, Shanghai Key Laboratory of Rare Earth Functional Materials, College of Chemistry and Materials Science, Shanghai Normal University, 200234 Shanghai, China. Correspondence and requests for materials should be addressed to D.Z. (email: dqzhang@shnu.edu.cn) or to H.L. (email: hexing-li@shnu.edu.cn)

Nano-sized semiconductors have been widely used as electrodes and photocatalysts in the application of energy and environmental field^{1–4}. However, without a favorable structure, they tend to suffer from some disadvantages such as the ease of aggregation and rapid photoelectron-hole recombination^{5–8}. The photosynthesis allows plants to harvest solar energy by converting it into carbohydrate molecules to fuel all biological life activities on Earth^{9–11}. Typically, photosynthesis efficiently occurs in the chloroplast (Fig. 1 left) with the nature designed non-continuously distributed components: the *Thylakoid* assembled by disk-like *Grana* is the site where light-dependent reactions take place and the layer-like *Stroma Lamella* links each *Thylakoid* by providing electron transport channels. Inspired by nature, great efforts have been devoted to designing binary, ternary, and multi-component hierarchical nanocomposites with synergistic effects^{12–17}. Among them, the carbon nanotubes (CNTs) are widely used since they usually display fascinating electrical and optical properties endowed by the unique 1-dimensional properties. Such properties are expected and advantageous for the surface reactions and charge transport processes^{18–22}. To decorate CNTs with semiconductors, the in-situ solvothermal strategy is reported^{21,23–25}. However, it is still hard to selectively control the growth sites of semiconductors on the CNTs and it is also difficult to avoid the free nucleation and growth. As we know, people can hardly realize the intimate contact between CNTs and nanocrystals.

We consider introducing microwave heating into the in situ fabrication involving CNTs, aiming to obtain the chloroplast structured photocatalysts enabled by microwave synthesis (Fig. 1 right). We infer that CNTs can selectively absorb microwaves and preferentially convert microwave energy into thermal energy with the formation of local super-hot dots, thus allowing and accelerating various organic/inorganic chemical reactions that occur on the CNTs surfaces. Because the geometry of CNTs presents a notably high aspect ratio of greater than 1000, the contacts between the ends of the long tubes are sufficient to create a conducting network. The remarkable electrical conductivity of CNTs at microwave frequencies also facilitates their use as broadband microwave-absorbing materials²⁶. As a typical example, the concept of solar-energy converter by constructing nano-rectenna solar cells using aligned CNTs as optical antennas is also introduced²⁷.

Here, our design is that CNTs would work as microwave antennas in the liquid–solid interfacial synthesis. By using CNTs

as microwave antennas, we have developed a general strategy for in-situ fabrication of semiconductors non-continuously threaded by the CNTs. As show in Fig. 1 (right), the synthesis was based on the idea of deploying 1-dimensional CNTs as a direct-charge transport superhighway. Taking advantage of the direct growth of photo-active semiconductors onto CNTs, a 3–dimensional conductive network with dual electron transfer pathways was obtained, which was very similar to the photosynthesis process in chloroplast. We have chosen one chloroplast structured photocatalyst of the non-continuously distributed and well-assembled single-crystal titanium oxides threaded by CNTs (CNT-TiO₂) to study their microwave synthesis mechanism, as well as their photocatalytic performances in nitric oxide oxidation reaction. This unique structure is proved for promoted light harvesting ability, while the 3–dimensional CNTs networks provided electron transfer pathways for accelerating chemical reactions. Thus, the as-synthesized CNTs-TiO₂ present a record-breaking efficiency of 86% for ultraviolet light-driven nitric oxide abatement. In addition, as a general strategy, a series of chloroplast structured nanomaterials can be synthesized and should be potentially used in the energy and environment fields.

Results

Morphology of the chloroplast structured photocatalyst. As a typical example, the CNT-TiO₂ was synthesized by heating the dimethyl sulfoxide (DMSO) solution containing TiCl₃ and CNTs with microwave. Transmission electron microscopy (TEM) images (Fig. 2a, b) demonstrated that the as-received sample consisted of uniform microspheres with an average diameter of approximately 500 nm threaded by CNTs. Both high-resolution transmission electron microscopy (HRTEM) and selected-area electron diffraction (SAED) images (Fig. 2c and inset) confirmed the single-crystalline nature of TiO₂ on the basis of well-resolved diffraction dots and the corresponding lattice spacing. Furthermore, the X-ray diffraction pattern (Fig. 2d) displayed sharp diffraction peaks characteristic of the pure anatase TiO₂ phase (JCPDF card No. 21–1272).

To examine the formation mechanism of such chloroplast structure, the CNT-TiO₂ was prepared by time-temperature-programmed process (Fig. 2e) and different samples obtained at desired heating times and temperatures were collected. The field emission scanning electron microscope (FESEM) images were shown in Fig. 2f–l. At the initial stage (microwave heating 7.5 min to 80 °C), only CNTs were observed in the FESEM images

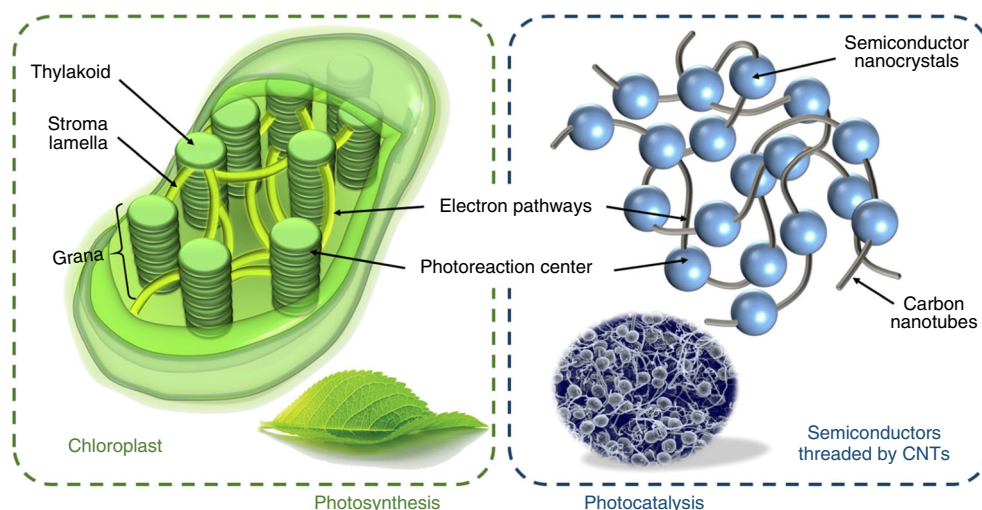


Fig. 1 The design principle of the chloroplast structured catalyst. Top view of chloroplast structure (left) and the architecture of the non-continuously distributed semiconductors threaded by CNTs (right)

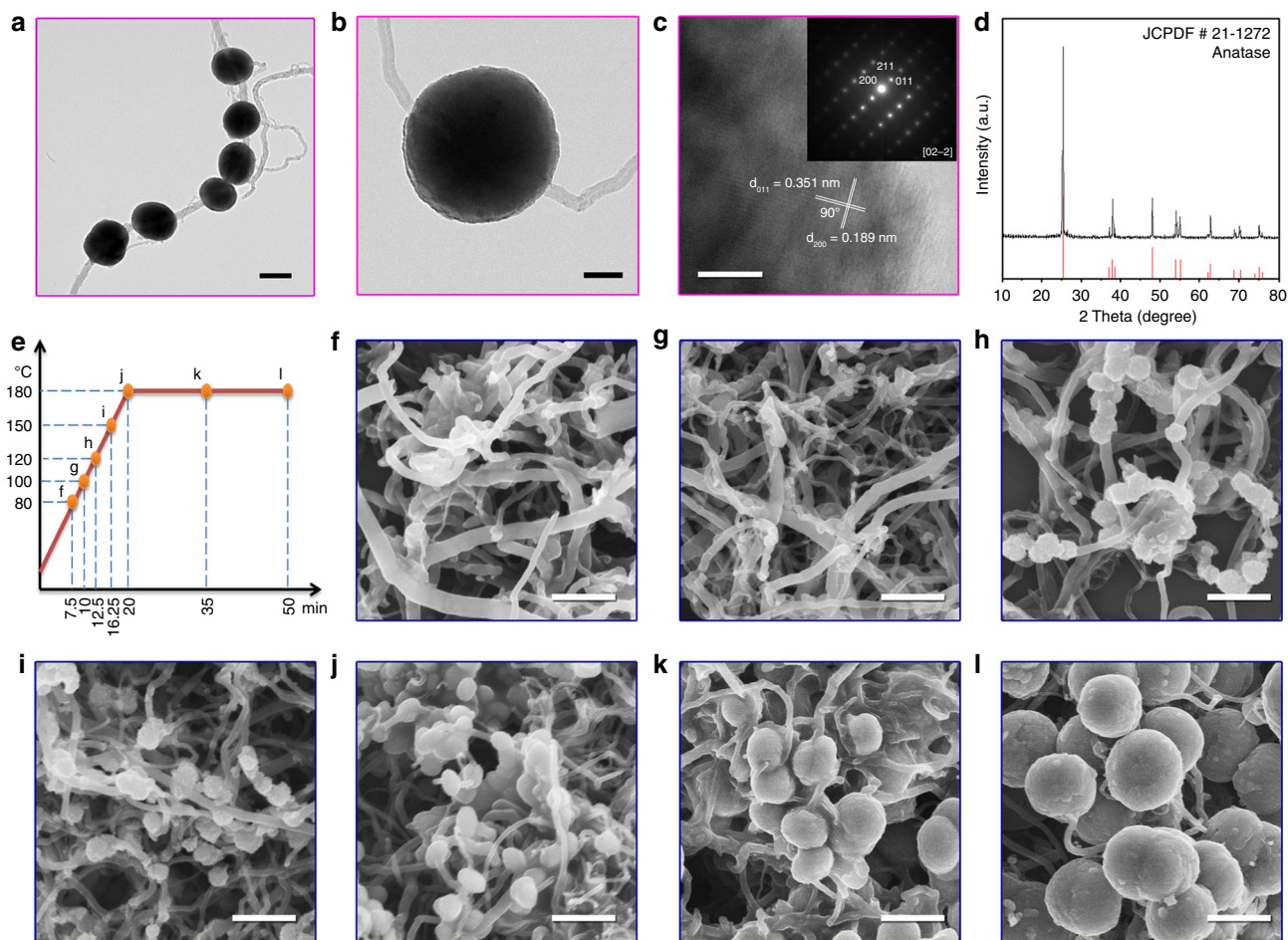


Fig. 2 Morphology and phase structure of chloroplast structured CNT-TiO₂. TEM images (**a**, **b**), HRTEM image with attached SAED pattern (**c**), and XRD pattern (**d**) of the as-prepared CNT-TiO₂. Different CNT-TiO₂ samples prepared at desired microwave-heating time and temperature (**e**) and their corresponding FESEM images (**f-l**). Scale bars in (**a**): 500 nm, (**b**): 100 nm, (**c**): 2 nm, and (**f-l**): 500 nm

(Fig. 2f), indicating that TiO₂ could not be formed on CNTs below 80 °C. As shown in Fig. 2g, when the microwave heating time was extended to 10 min with temperature reaching up to 100 °C, small nanoparticles were deposited onto the CNTs surface due to the formation of TiO₂ nanocrystals. Figure 2h–j revealed that further increasing microwave heating time to 20 min with the temperature reaching up to 180 °C resulted in more TiO₂ nanocrystals onto the CNTs surface which is determined as the crystal nucleation process. By keeping at 180 °C, increasing the microwave-heating time from 0 to 30 min caused significant increase in the particle size of TiO₂ nanocrystals from Fig. 2j–l.

It is worth mentioning that this synthesis method is generic and can be applied to different materials. A series of nanocomposites with chloroplast structure has been prepared including CNT-CeO₂, CNT-Mn₃O₄, CNT-Cu₂O, CNT-ZIF-67, and CNT-ZIF-8 (see the FESEM images in Supplementary Fig. 1 and the XRD patterns in Supplementary Fig. 2).

Photocatalytic removal of nitric oxide. As CNTs could promote electron transport in nanocomposites, they could work as co-catalysts or additives and should have considerable applications in a series of fields^{28–32}. The CNT-TiO₂ microspheres (CT, shown in Fig. 3a) were used as catalysts in the photocatalytic NO oxidation to evaluate the advantages of this unique chloroplast structure. Besides, the completely encapsulated core-shell structure of CNT-TiO₂ (f-CT, shown in Fig. 3b), as well as the mechanical mixing of CNTs and TiO₂ microsphere (CT-mx,

shown in Fig. 3c) could also be prepared as the references. As illustrated in Fig. 3d, in the gas-phase flow photocatalytic NO oxidation reaction, the CT sample showed a remarkable high NO conversion rate of ~86% under UV-light irradiation and desirable reaction stability. To the best of our knowledge, this is the record-breaking photocatalytic NO conversion among all the UV-response catalysts (e.g., O_v-TiO₂ at ~20%³³, single atom Pd-TiO₂ at ~47%³⁴, g-C₃N₄-TiO₂ at ~56%³⁵, PtO_x-TiO₂ at 71%³⁶ and C, N-doped P25 TiO₂ at 79.6%³⁷). While, the f-CT exhibited the lower conversion of ~77% after equilibrium in 20 min, but gradually dropped to ~58% after 120 min irradiation, which was even much lower than that for sample CT-mx (~72%). Considering that these samples own the similar CNT/TiO₂ ratio, surface area and light absorption properties analyzed in Supplementary Fig. 3, the difference in photocatalytic performance could be considered as their different charge transport properties. Thus, the photocurrent, electrochemical impedance tests, charge dynamic analysis, as well as the scheme illustration were shown and discussed in Fig. 3e–h to understand the photo-excited carriers' separation and transport processes. For the CT and f-CT, microwave synthesis created an intimate contact between CNTs and TiO₂ by the covalent bonds of Ti–O–C=O or Ti–O–C (located at ~1120 cm⁻¹) formed due to the etherification process between the CNTs surface carboxyl/hydroxyl groups and TiO₂, which was evidenced by the Fourier transform infrared (FT-IR) spectra as shown in Supplementary Fig. 4. With this kind of strong “line-contact”

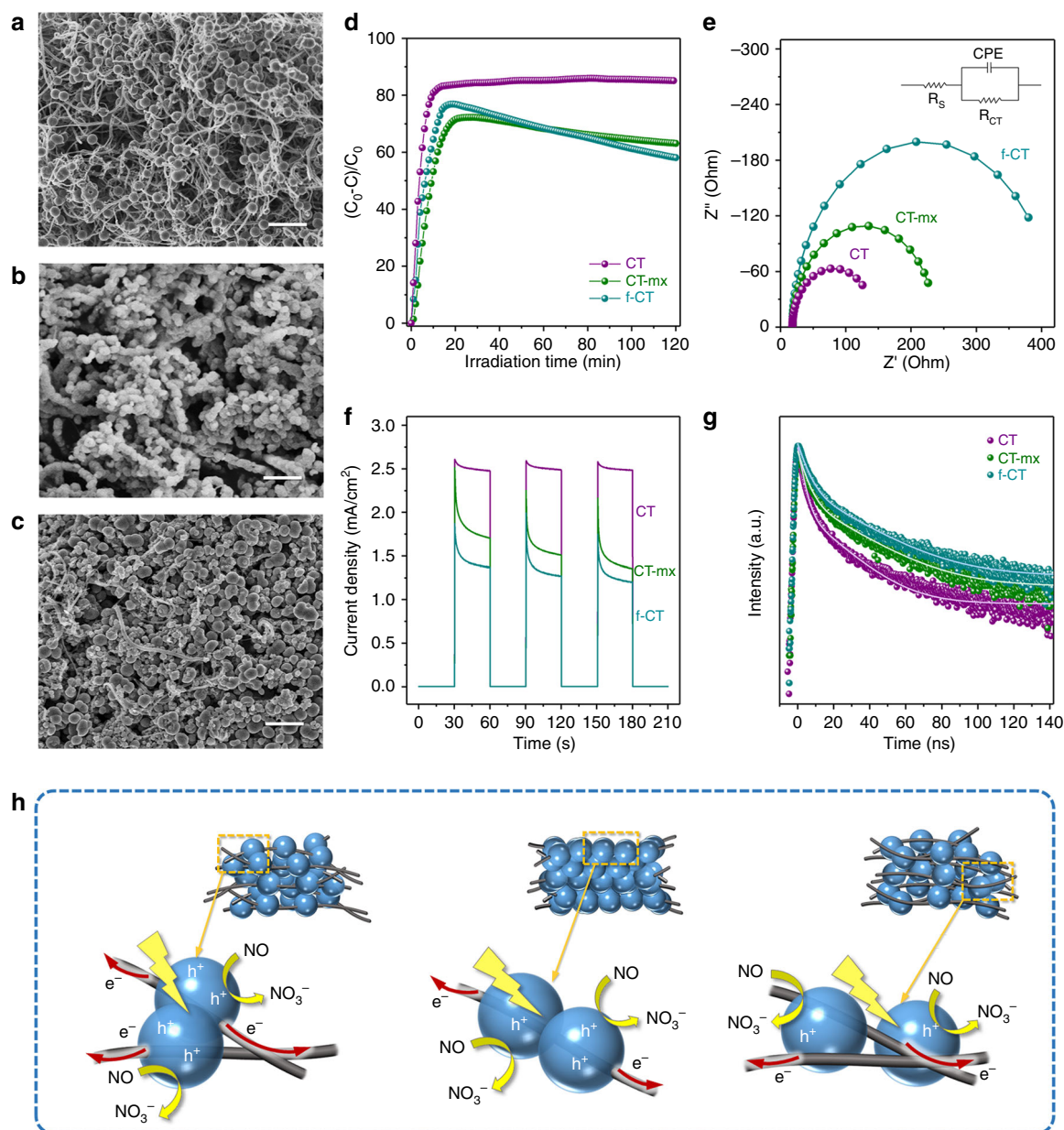


Fig. 3 Chloroplast structure of CNT-TiO₂ catalysts facilitated the electron transport and enhanced the photocatalytic NO oxidation performance. SEM image of different CNT-TiO₂ composites: **(a)** CT, **(b)** f-CT and **(c)** CT-mx. **d** UV-light-driven photocatalytic NO oxidation performances, **(e)** electrochemical impedance spectra (EIS) with the equivalent circuit model in the inset, **(f)** photocurrent spectra and **(g)** time-resolved transient photoluminescence decay profiles of sample CT, f-CT, and CT-mx. **h** The scheme illustration of the morphologies and photo-carriers separation process of sample CT, f-CT, and CT-mx. Scale bars in **a–c**: 2 μm

(shown in Fig. 3h, left and middle) rather than the weak “point-contact” in CT-mx (shown in Fig. 3h right), the photo-excited electron could be separated rapidly, thus resulting in the remarkably high performances in NO removal and high densities of photocurrent. The electrochemical impedance data (EIS) were simulated base on the Randles equivalent circuit model (shown in Fig. 3e and the inset). The circuit included a solution resistance (R_s), charge transfer impedance (R_{CT}) and a non-ideal capacitor (CPE), which substituted the double layer capacitance of the electrode–electrolyte interface. The capacitor is related to the adsorption of reactant on the surface of electrode and the diffusion process associated with charge transfer reaction across the electrode–electrolyte interface. The charge transfer impedance (R_{CT}) of CT, CT-mx, and f-CT were distinguished and could be fitted to 126.4, 218.9, and 400.2 Ω ,

respectively. For the CT and CT-mx samples, they exhibited lower R_{CT} value in the EIS spectra and relatively higher photocurrents shown in Fig. 3f. This is attributed to 3-dimensional conductive networks in topologies constructed by the crossing linked CNTs (shown in Fig. 3h left) which promoted a better electric conductivity and provided index increasing pathways for independent electron transport. Meanwhile, the time-resolved transient photoluminescence decay profiles were shown in Fig. 3g (detail fitted parameters shown in Supplementary Table 1). The average emission life-time of CT (9.2 ns) was shorter than that of CT-mx (13.6 ns) and f-CT (14.8 ns). The observed difference in mean lifetimes was due to the number of effective interfaces between TiO₂ and CNTs. For the sample of CT, multiple interfaces between TiO₂ and CNTs provided relatively efficient electron transfer resulting in a short

lifetime. While, the aggregation of TiO₂ particles might suppress the interfacial electron transfer from TiO₂ to CNT, thus resulting in the prolonged lifetime for the f-CT sample. Furthermore, the photocarrier density calculated from the Mott–Schottky plots (Supplementary Fig. 5) also confirmed that such chloroplast structure successfully prolonged the life-time of photogenerated carriers, thus presenting enhanced activities in NO oxidation. However, in sample f-CT, there existed less interaction between each CNTs as a result of conductivity decrease because the CNTs were completely wrapped by semiconductor TiO₂ (as shown in Fig. 3h middle). Although the sample f-CT showed the high activity and high photocurrent in the initial stage, the lack of topological conductive networks finally resulted in the rapid recombination of photo-carriers further led to their dramatically drop in the long run. Therefore, we think different photogenerated charge kinetics over various samples also caused the different selectivity of NO₃⁻ and NO₂ product in the NO oxidation reaction. Such hypothesis was supported by Supplementary Fig. 6, which showed the concentration profiles of NO and NO₂ during the photocatalytic NO oxidation reaction when different catalysts were applied. After analyzing the real-time NO and NO₂ concentration, the NO₂ selectivity in 2 h could be 4.5%, 6.8%, and 1.2% for CT-mx, f-CT, and CT, respectively, indicating that fast carrier separation kinetics over the CT sample promoted the high concentration of reactive holes to realize deeply oxidation of NO to NO₃⁻ instead of NO₂.

The formation of localized “super-hot” dots on CNTs. The CNTs played a key role in fabricating chloroplast structured nanomaterials. As well-known, the loss tangent ($\tan \delta$) is an intrinsic parameter used to define the ability of a specific material or solvent to convert microwave energy into heat³⁸. The $\tan \delta$ value can be expressed as $\tan \delta = \epsilon''/\epsilon'$, where ϵ' refers to the polarizability and ϵ'' is the dielectric loss corresponding to the efficiency to convert the microwave energy into heat^{39,40}. Different materials exhibit different $\tan \delta$ at a given microwave frequency and temperature. The CNTs have an excellent high $\tan \delta$ of 1.45 at a frequency of 2.45 GHz and room temperature⁴¹, which is much more positive than that of many solvents (e.g., acetone = 0.054, water = 0.123, DMF = 0.161, methanol = 0.659, and DMSO = 0.825)³⁸. Thus, the CNTs could act as microwave antennas to efficiently absorb microwave and subsequently convert microwave energy into thermal energy, leading to the formation of surface “super-hot” dots with much higher temperature than that of bulk solution^{42–45}. Unfortunately, we could not directly measure the local surface temperature to confirm the “super-hot” dots on CNTs. Under this case, we determined the DMSO solution temperature by heating the system in the presence or absence of CNTs and observed the variation of the solution temperature. As shown in Fig. 4a, the DMSO solution containing CNTs exhibited a substantially fast heating rate that resulted in a higher solution temperature than that of the pure DMSO solution. However, the solution containing polytetrafluoroethylene (PTFE) with low $\tan \delta$ (~0.002 at 2.45 GHz)

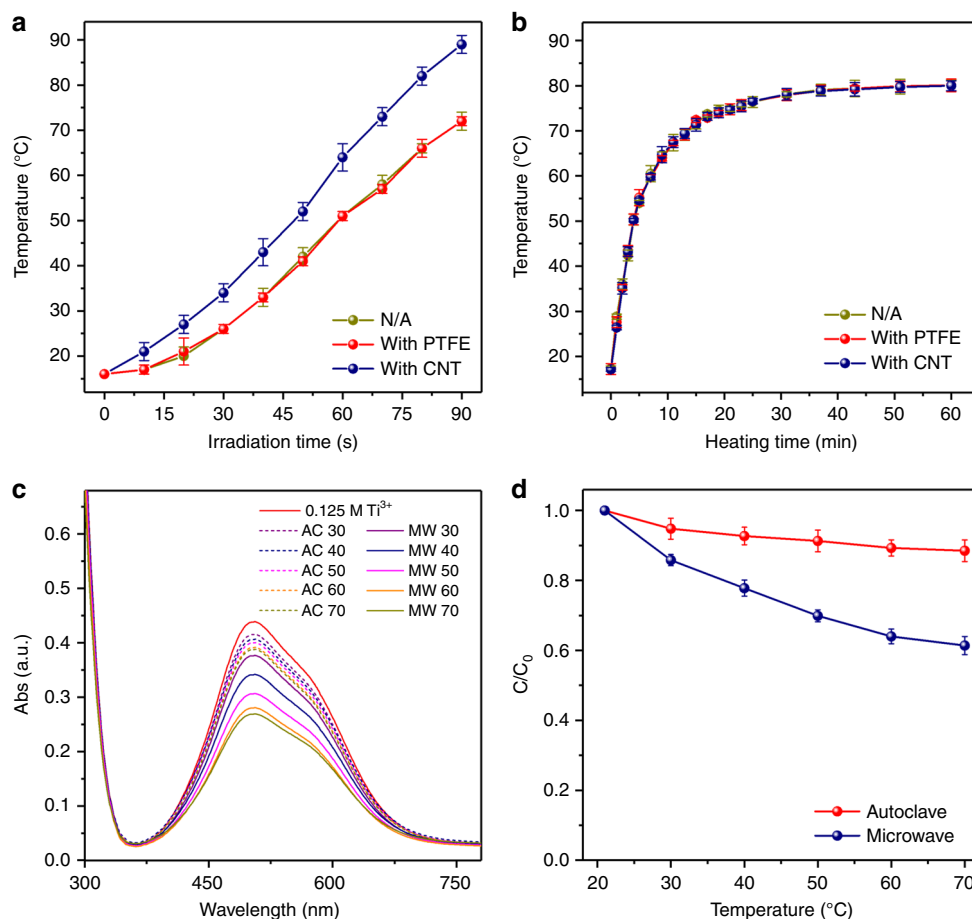


Fig. 4 Microwave effects on CNTs. Plots of the temperature of DMSO solution (200 mL) vs. heating time in the presence or absence of CNTs and PTFE (100 mg) with the heating source of **(a)** microwave irradiation (800 W) and **(b)** oil bath (90 °C). The Ti³⁺ adsorption properties of CNTs: **(c)** UV-Vis spectra of TiCl₃ solution and **(d)** temperature-dependent concentration change of Ti³⁺ under microwave irradiation and autoclave hydrothermal heating by keeping the specific temperature for 20 min

exhibited nearly the same temperature as the pure DMSO solution. The enhanced heating rate of solution in the presence of CNTs was caused by the heat transfer from CNTs to solution based on the much higher temperature on the CNTs surfaces. In contrast, when the regular oil-bath heating was used instead of microwave, the DMSO solution containing CNTs or PTFE exhibited the similar temperature as the pure solution (see Fig. 4b). It indicated that traditional heating transfer could hardly be affected by the additives in solution. To sum up the above, the CNTs with much higher $\tan \delta$ could work as microwave collectors and converters in solution via the localized “super-hot” dots under the specific electromagnetic wave irradiation which facilitated the localized nucleation and growth of TiO_2 crystal on CNTs instead of solution during the synthesis.

Designated adsorption of metal-ions on CNTs. To form the chloroplast structures, the localized Ti^{3+} adsorption was also important. As is confirmed by the metal-ion adsorption test in Fig. 4c, d, we also believed the microwave favored the adsorption of Ti^{3+} by oxygen-contained functional groups (carboxyl or hydroxyl) on CNTs from the bulk solution. UV-Vis was used to track the concentration of Ti^{3+} since the absorbance in the 505 nm wavelength is the standard Ti^{3+} signal. Figure 4c demonstrated the UV-Vis spectra of 0.125 M TiCl_3 solution before and after keeping on the temperature from 30 °C to 70 °C for 20 min under both microwave irradiation and regular hydrothermal autoclave. The corresponding temperature-dependent solution concentration change was shown in Fig. 4d, which clearly exhibited that the CNTs showed higher Ti^{3+} adsorption capability under microwave heating than that under regular hydrothermal heating at the same temperature. Meanwhile, increasing microwave heating temperature (more microwave energy absorbed by CNTs) led to the significant enhance in Ti^{3+} adsorption since the concentration of Ti^{3+} solution dropped from 85.5% (30 °C) to 61.4% (70 °C). However, in the autoclave hydrothermal condition, the adsorption amount just showed a slightly enhance with increasing the temperature. Thus, microwave could also enhance the ability for CNTs to adsorb metal-ions and induce their localized hydrolysis on the surface of CNTs. In addition, the CNTs also lowered the nucleation temperature of TiO_2 crystal. As shown in Supplementary Fig. 7, by microwave heating TiCl_3 in DMSO solution for 10 min to 100 °C, the solution remained original yellow color and no significant solid products were found. It suggested that the hydrolysis reaction of TiCl_3 could not occur at such low temperature in this case. On the contrary, in the similar process with CNTs added, the yellow solution became much lighter, accompanied by the formation of gray powders at the bottom. The gray powder can be further confirmed by the FESEM image of Supplementary Fig. 8a. On the surface of the CNT, the bright spots in red circles may be the nuclei of TiO_2 crystal. Meanwhile, we also found that, when the TiCl_3 hydrolysis reaction was carried out at 100 °C via regular oil-bath heating, no significant reaction occurred even in the presence of CNTs as shown in the Supplementary Fig. 7 and Supplementary Fig. 8b because no surface change could be observed. These results demonstrated that, under microwave heating, the temperature of the CNTs' surface should be much higher than that in the bulk solution and was sufficiently high for the hydrolysis of Ti^{3+} into TiO_2 . Thus, the TiO_2 nanocrystals formed only on the CNTs surface rather than in the bulk solution. To further confirm this hypothesis, we also used a 1-dimensional polytetrafluoroethylene (PTFE) with a very low $\tan \delta$ as a reference material instead of CNTs. From the FESEM of PTFE- TiO_2 (shown in Supplementary Fig. 9), we observed that only very few TiO_2 nanocrystals growing on the PTFE surface after the precursor was microwave-heated to

180 °C and maintained for 30 min. This was obviously due to PTFE's poor ability for absorbing microwave energy to generate local “super-hot” dots, while the CNTs surface could initiate the hydrolysis of adsorbed Ti^{3+} due to the localized high temperature, leading to the in situ formation and assembly of TiO_2 nanocrystals along them.

The role of CNTs surface functional group. The presence of polar groups like carboxyl (–COOH) and hydroxyl (–OH) on CNTs also played a vital role in this microwave reaction mainly from the following two aspects: first, oxygen-contained groups promoted the microwave absorbance and conversion of CNTs due to the enhanced dielectric property by increased polarizability which lead to the formation of more “super-hot” dots in the Joule heating process;⁴⁶ second, the surface –COOH and –OH could work as the active absorption sites for metal-ions to ensure the localized nucleation and growth of nanocrystals. According to the phenomenological model⁴⁷, the CNTs might undergo a highly efficient superheating process through transformation of electromagnetic energy into mechanical vibrations because of the presence of polar groups connected with the six-membered-ring carbon backbone to form dangling bonds. These dangling bonds, together with the CNTs, resulted in the enhanced absorbance of microwaves and the subsequent conversion of the absorbed microwave energy into thermal energy, leading to the abrupt increase of the CNTs' surface temperature. It could be confirmed by comparing the solution heating rate by adding CNTs with different acid treatment time (detailed method described in the supporting information). As the Fourier-transform infrared (FT-IR) spectra (Fig. 5a) revealed, the amounts of –COOH and –OH groups covalently bonded to the CNTs increased with the prolonging of HNO_3 -pretreating time from 30 min to 240 min. As shown in Fig. 5b, more oxygen-contained group resulted in the significantly increasing heating rate of the solution. Moreover, pre-treatment enhanced the metal-ion adsorption illustrated in Fig. 5c. By fixed the microwave/autoclave temperature in 50 °C, the Ti^{3+} concentrations remaining in solution were compared. Although the acid treatment on CNTs enhanced the Ti^{3+} adsorption by regular autoclave hydrothermal to a certain degree, the increasing rate by microwave was much more considerable and obvious. Interestingly, the CNT-A120 and CNT-A240 presented the similar temperature raising phenomenon, as well as ion adsorption property. It was because that the surface functional group tended to be saturation after 120 min of pre-treatment, thus further acidification had less effect on the surface property of CNTs.

Accordingly, by well controlling the surface oxygen-contained groups, we could continuously adjust the density of TiO_2 nanospheres threaded by CNTs from the non-continuous distribution state to the completely encapsulated core-shell structure shown in Supplementary Fig. 10. In addition, other CNT- TiO_2 nanocomposites with hierarchical morphologies could also be synthesized based on the present microwave-antenna strategy (see the experimental details in the Supporting Information), showing its universality. The FESEM images in Fig. 5d–i displayed anatase TiO_2 nanocubes with exposed (001) and (010) facets, anatase TiO_2 nanodecahedrons with exposed (001) and (101) facets, rutile TiO_2 nanoflowers (see the XRD patterns in Supplementary Fig. 11) threaded by untreated CNTs (d) (e) (f) and CNTs with acid treated for 240 min (g) (h) (i). We also compared the FESEM images of the TiO_2 in anatase microspheres, rutile nanoflowers and anatase nanodecahedrons obtained via autoclave hydrothermal and microwave route in the presence or absence of CNTs, respectively (see Supplementary Fig. 12). When regular autoclave hydrothermal heating was used,

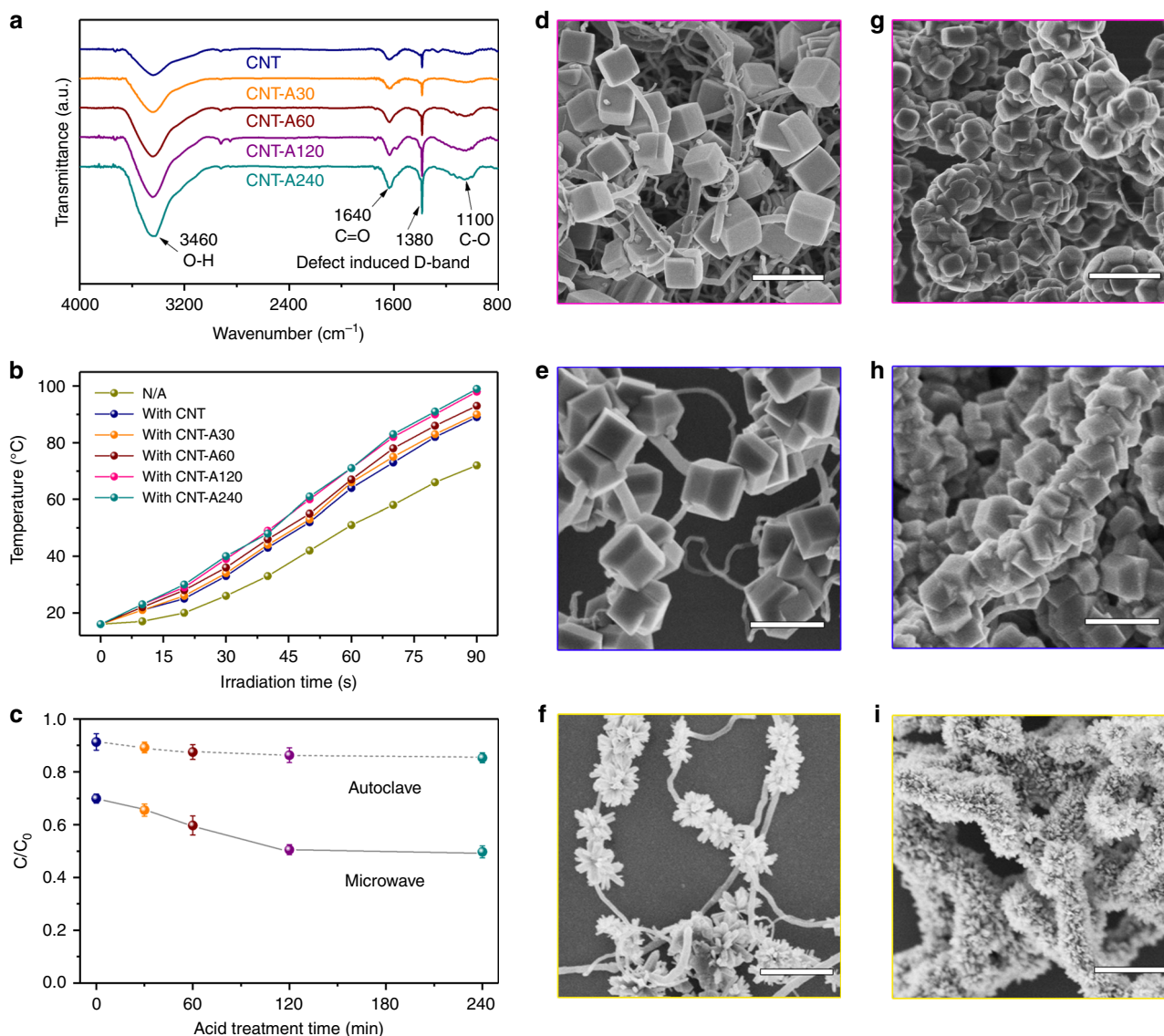


Fig. 5 Surface functional groups affected the microwave antenna performance of CNTs. **a** FT-IR spectra of CNTs after HNO_3 pre-treatment for 0, 30, 60, 120 and 240 min. **b** Plots of the temperature of DMSO solution (200 mL) vs. microwave irradiation time in the presence or absence of different CNTs. **c** CNTs acid pre-treatment time-dependent concentration change of Ti^{3+} under microwave irradiation and autoclave hydrothermal heating by keeping the heating temperature of 50°C for 20 min. **d-i** FESEM images of (**d, g**) CNT-anatase TiO_2 nanocrystals with exposed (001) and (010) facets, (**e, h**) CNT-threaded anatase TiO_2 nanodecahedrons with exposed (001) and (101) facets, and (**f, i**) CNT-threaded rutile TiO_2 nanoflowers by using (**d-f**) untreated and (**g-i**) CNTs pre-treated with HNO_3 for 240 min. Scale bars in **d-i**: 1 μm

the TiO_2 obtained with and without CNTs exhibited similar morphologies, and no direct growth of TiO_2 nanoparticles on the CNTs' surface was observed. This was due to the autoclave conduction heating mode which made the solution temperature to be higher than that of CNTs in the initial stage since the heat was transferred from the outside to the inside in the autoclave system. Therefore, the nucleation site could be in the solution rather than on the CNTs' surfaces. However, with the application of microwave instead of regular hydrothermal heating, the TiO_2 samples obtained with and without CNTs exhibited remarkably different morphologies. In the absence of CNTs, only randomly dispersed TiO_2 nanoparticles were observed in the solution. Only by satisfying the two conditions of microwave heating and the presence of CNTs, the chloroplast structure nanohybrids could be prepared. These results further confirmed the nature of CNTs working as microwave antenna, converting more energy into the

heat and being the nucleation sites for direct growth of TiO_2 crystals. At the same time, because of the CNTs' outstanding electrical and mechanical characteristics, such as their high surface area, desirable volume ratio and the intrinsic metallic character (CNT larger than 2 nm in diameter), they could also efficiently avoid aggregation of the TiO_2 nanoparticles, corresponding to a uniform shape with small particle size compared with those obtained in the absence of CNTs⁴⁸.

Discussion

At this point, we could summarize the microwave antennas mechanism of the in situ fabricating chloroplast structured CNTs-threaded TiO_2 nanocrystals illustrated in Fig. 6a. At the initial stage, the CNTs could strongly absorb electromagnetic wave like microwave antennas and then convert the microwave

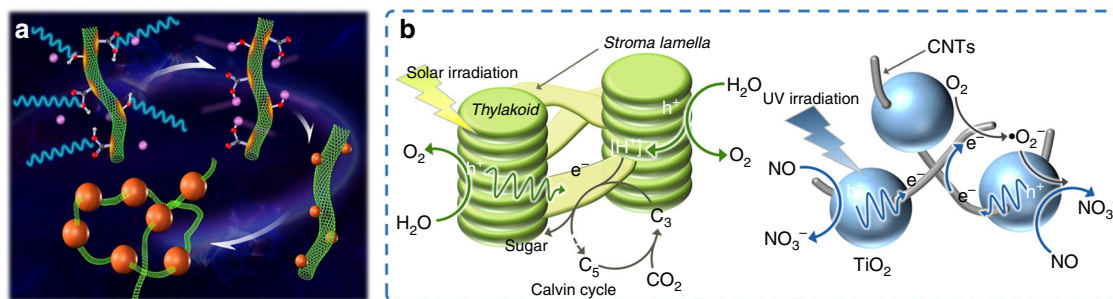


Fig. 6 The mechanism illustration for CNTs as microwave antennas and chloroplast structures in photosynthesis as well as photocatalysis. **a** Schematic illustration of the CNT-TiO₂ preparation process: microwave absorbing and converting into super-hot dots (red dots), Ti³⁺ ions (purple dots) adsorption onto super-hot dots, Ti³⁺ hydrolysis into TiO₂ crystal seeds (small brown dots), and TiO₂ nanocrystals (big brown dots). **b** The photosynthesis mechanism of chloroplast (left) and the photocatalytic NO removal mechanism of chloroplast structured CNTs-TiO₂

energy into heat to generate “super-hot” dots on their surface (red dots). These “super-hot” dots favored adsorption of Ti³⁺ ions (purple dots) by carboxyl or hydroxyl groups. When the surface “super-hot” dots reached the nucleation temperature, the Ti³⁺ could hydrolyze into nuclei seeds (small brown dots) on the CNTs. Finally, with the increase of microwave time and temperature, more “super-hot” dots on the CNTs surface generated, which could absorb more Ti³⁺ ions, followed by hydrolyzing into more nuclei seeds of TiO₂. The nuclei further grew into TiO₂ nanocrystals (big brown dots) and finally formed the chloroplast structure. In this synthesis of CNTs-TiO₂ nanocomposites, after microwave-heating for 20 min with the corresponding temperature in 180 °C, the density of TiO₂ nanocrystals on the CNTs surface reached maximum. Further increasing microwave-heating time, the temperature could not increase the adsorption of Ti³⁺ ions onto CNTs surface due to the spatial hindrance. Further prolonging the microwave-heating time resulted in crystal growth, leading to the increased size of TiO₂ nanocrystals as shown in Fig. 2j–l.

By mimicking the photosynthesis process in chloroplast, the as-obtained chloroplast structured CT sample exhibited the highest and most stable photocatalytic NO conversion performance, and its photocatalytic mechanism was similar with the photosynthesis in chloroplast. As illustrated in Fig. 6b, in photosynthesis the light-dependent reactions occur in the disk-like *Grana* assembled *Thylakoid*, where H₂O can be oxidized to O₂ by the photogenerated holes through photosystem I and II with the formation of proton (H⁺). While, the layer-like *Stroma Lamella* links each *Thylakoid* by providing electron/H⁺ transport channels to promote the Calvin cycle for efficient capturing of CO₂ to produce sugar. In the photocatalytic NO removal reaction, as the light-dependent reaction, the CT sample with the chloroplast structure can be excited by UV light with generated holes in TiO₂ microsphere to deeply oxidize NO to NO₃⁻ (confirmed by the UV-vis analysis in Supplementary Fig. 13). As shown in Supplementary Fig. 13c, the NO₃⁻ production over the CT sample increased with the irradiation time. As mentioned before, the NO₃⁻ selectivity could be more than 98% over the sample CT. After 2 h reaction, the accumulated HNO₃ on the catalyst surface did not affect the stability of the catalyst due to the enough adsorption sites for NO₃⁻. This also could be ascribed to the fast carrier separation kinetics over the CT sample which could promote the high concentration of reactive holes to release deep oxidation of NO to NO₃⁻ instead of NO₂. Furthermore, less NO₂ adsorption also made this catalyst more stable than the other two catalysts. The intimate “line-contact” between CNTs and TiO₂ microsphere, as well as the constructed 3-dimensional CNTs

conductive networks facilitate the photo-carriers’ separation. With the negative reduction potential, the accumulated electrons on the CNTs reacting with O₂ can induce the formation of •O₂⁻ species. This was confirmed by the electron spin resonance results as shown in Supplementary Fig. 14. Such active species can further benefit the oxidation reaction to realize the record-breaking performance.

In conclusion, by mimicking chloroplast towards efficient charge transport, we have developed a general microwave-antenna strategy for in situ synthesizing non-continuous distribution of nano-semiconductors threaded by CNTs. The 1-dimensional materials of CNTs with strong ability for absorbing microwave were used as microwave antennas to generate the high-temperature local surface “super-hot” dots. Such “super-hot” dots would induce adsorption, hydrolysis or coordination of metallic ions, followed by nucleation, crystal-growth and self-assembly into a unique architecture with metal oxides and metal organic frameworks (MOFs) nanocrystals threaded by CNTs. In CNT-TiO₂ nanocomposites, like chloroplast, the cross-linked CNTs provided electron conducting pathways facilitating enhanced photocatalytic performance in the gas-phase reaction. This new microwave-antenna strategy can be extended to in situ fabrication of other 1-dimensional binary or ternary nanocomposites and even 2-dimensional or 3-dimensional chloroplast structured nanocomposites with controllable architectures like those found in nature, which may offer more opportunities for their applications in environmental and energy fields.

Methods

Synthesis of CNT-TiO₂ with anatase microspheres (sample CT). In a typical synthesis, 20 mg CNTs were dispersed in 18 mL dimethyl sulfoxide (DMSO, Aladdin) for 30 min to form a black suspension in an ultrasonic cleaner. As references, CNTs with different acid treatment time were used instead of the CNT without acid treatment. Then, 2 mL 15 wt% TiCl₃ aqueous solution with 10–15 wt% HCl (Merck-Schuchardt) was added to the suspension with magnetic stirring for 10 min. Subsequently, the mixture was moved to a 40 ml quartz vessel with a Teflon lid. It was treated at 180 °C for 30 min with a heating rate of 15 °C min⁻¹ and with an initial pressure of 35 bar by N₂ in a single chamber microwave digestion system (Ultrawave, Milestone). The resulting powder was washed with deionized water and absolute ethanol for 3 times, followed by vacuum drying at 80 °C for 4 h.

Photocatalytic NO oxidation activity test. The photocatalytic NO oxidation in gas phase was carried out at ambient temperature in a continuous flow reactor with volume of 10.8 L (36 × 20 × 15 cm). For UV lights driven photocatalysis, eight of UV lamps (6w, 365 nm) located vertically above the reactor was used as light source. In each run of experiments, an air gas flow containing 500 ppb NO was allowed to pass through 0.20 g photocatalyst at the flow velocity of 4.0 L/min. After reaching adsorption-desorption equilibrium on the photocatalyst, the lamp was turned on to start the photocatalysis reaction. The concentration of

NO was continuously measured by using a chemiluminescence NO analyzer (Thermo Environmental Instruments Inc. Model 42i). The NO removal rate (%) was calculated based on the following equation: NO removal rate (%) = $(C_0 - C)/C_0 \times 100\%$, where C_0 and C refer to the NO concentration determined before and after reaction.

Data availability

The data that support the findings of this study are available from the corresponding authors upon reasonable request.

Received: 16 August 2018 Accepted: 15 March 2019

Published online: 05 April 2019

References

- Schrauben, J. N. et al. Titanium and zinc oxide nanoparticles are proton-coupled electron transfer agents. *Science* **336**, 1298–1301 (2012).
- Koppens, F. H. L. et al. Photodetectors based on graphene, other two-dimensional materials and hybrid systems. *Nat. Nanotech* **9**, 780–793 (2014).
- Kim, H. et al. Water harvesting from air with metal-organic frameworks powered by natural sunlight. *Science* **356**, 430–432 (2017).
- Cha, E. et al. 2D MoS₂ as an efficient protective layer for lithium metal anodes in high-performance Li-S batteries. *Nat. Nanotech* **13**, 337–344 (2018).
- Simon, T. et al. Redox shuttle mechanism enhances photocatalytic H₂ generation on Ni-decorated CdS nanorods. *Nat. Mater.* **13**, 1013–1018 (2014).
- Shin, S. S. et al. Colloidally prepared La-doped BaSnO₃ electrodes for efficient, photostable perovskite solar cells. *Science* **356**, 167–171 (2017).
- Welin, E. R., Le, C., Arias-Rotondo, D. M., McCusker, J. K. & MacMillan, D. W. C. Photochemistry photosensitized, energy transfer-mediated organometallic catalysis through electronically excited nickel(II). *Science* **355**, 380–384 (2017).
- Liao, L. et al. Efficient solar water-splitting using a nanocrystalline CoO photocatalyst. *Nat. Nanotech* **9**, 69–73 (2014).
- Zhang, T. & Lin, W. Metal-organic frameworks for artificial photosynthesis and photocatalysis. *Chem. Soc. Rev.* **43**, 5982–5993 (2014).
- McCormick, T. M. et al. Reductive side of water splitting in artificial photosynthesis: new homogeneous photosystems of great activity and mechanistic insight. *J. Am. Chem. Soc.* **132**, 15480–15483 (2010).
- Maeda, K. et al. Photocatalytic overall water splitting promoted by two different cocatalysts for hydrogen and oxygen evolution under visible light. *Angew. Chem. Int. Ed.* **49**, 4096–4099 (2010).
- Kim, D., Sakimoto, K. K., Hong, D. & Yang, P. Artificial photosynthesis for sustainable fuel and chemical production. *Angew. Chem. Int. Ed.* **54**, 3259–3266 (2015).
- Pan, D. et al. Efficient photocatalytic fuel cell via simultaneous visible-photoelectrocatalytic degradation and electricity generation on a porous coral-like WO₃/W photoelectrode. *Environ. Sci. Technol.* <https://doi.org/10.1021/acs.est.8b05685> (2019).
- Douglas, T. A bright bio-inspired future. *Science* **299**, 1192–1193 (2003).
- Cho, I. et al. Codoping titanium dioxide nanowires with tungsten and carbon for enhanced photoelectrochemical performance. *Nat. Commun.* **4**, 1723 (2013).
- Xiao, S. et al. Copper nanowires: a substitute for noble metals to enhance photocatalytic H₂ generation. *Nano Lett.* **15**, 4853–4858 (2015).
- Xiao, S. et al. Porous CuO nanotubes/graphene with sandwich architecture as high-performance anodes for lithium-ion batteries. *Nanoscale* **8**, 19343–19351 (2016).
- Kim, Y. K. & Park, H. Light-harvesting multi-walled carbon nanotubes and CdS hybrids: application to photocatalytic hydrogen production from water. *Energy Environ. Sci.* **4**, 685–694 (2011).
- Wang, Z., Luan, D., Madhavi, S., Hu, Y. & Lou, X. Assembling carbon-coated alpha-Fe₂O₃ hollow nanohorns on the CNT backbone for superior lithium storage capability. *Energy Environ. Sci.* **5**, 5252–5256 (2012).
- Li, H. et al. A flexible CdS nanorods-carbon nanotubes/stainless steel mesh photoanode for boosted photoelectrocatalytic hydrogen evolution. *Chem. Commun.* **55**, 2741–2744 (2019).
- Gong, M. et al. An Advanced Ni-Fe Layered double hydroxide electrocatalyst for water oxidation. *J. Am. Chem. Soc.* **135**, 8452–8455 (2013).
- De Volder, M. F. L., Tawfik, S. H., Baughman, R. H. & Hart, A. J. Carbon nanotubes: present and future commercial applications. *Science* **339**, 535–539 (2013).
- Hu, L. et al. Symmetrical MnO₂-carbon nanotube-textile nanostructures for wearable pseudocapacitors with high mass loading. *ACS Nano* **5**, 8904–8913 (2011).
- Liang, Y. et al. Oxygen reduction electrocatalyst based on strongly coupled cobalt oxide nanocrystals and carbon nanotubes. *J. Am. Chem. Soc.* **134**, 15849–15857 (2012).
- Wang, D. et al. Highly active and stable hybrid catalyst of cobalt-doped Fe₂S nanosheets-carbon nanotubes for hydrogen evolution reaction. *J. Am. Chem. Soc.* **137**, 1587–1592 (2015).
- Kappe, C. O., Stadler, A. & Dallinger, D. *Microwaves in Organic And Medicinal Chemistry*. (Wiley-VCH, Weinheim, 2012).
- Bailey, R. L. A proposed new concept for a solar-energy converter. *J. Eng. Power* **94**, 73–77 (1972).
- Wang, J., Wang, Z. & Zhu, Z. Synergetic effect of Ni(OH)₂ cocatalyst and CNT for high hydrogen generation on CdS quantum dot sensitized TiO₂ photocatalyst. *Appl. Catal. B-Environ.* **204**, 577–583 (2017).
- Nardecchia, S., Carriazo, D., Luisa Ferrer, M., Gutierrez, M. C. & del Monte, F. Three dimensional macroporous architectures and aerogels built of carbon nanotubes and/or graphene: synthesis and applications. *Chem. Soc. Rev.* **42**, 794–830 (2013).
- Wang, D. et al. Highly active and stable hybrid catalyst of cobalt-doped Fe₂S nanosheets-carbon nanotubes for hydrogen evolution reaction. *J. Am. Chem. Soc.* **137**, 1587–1592 (2015).
- Liu, Q. et al. Carbon nanotubes decorated with CoP nanocrystals: a highly active non-noble-metal nanohybrid electrocatalyst for hydrogen evolution. *Angew. Chem. Int. Ed.* **53**, 6710–6714 (2014).
- Li, D. et al. Molybdenum sulfide/N-doped cnt forest hybrid catalysts for high-performance hydrogen evolution reaction. *Nano Lett.* **14**, 1228–1233 (2014).
- Nakamura, I. et al. Role of oxygen vacancy in the plasma-treated TiO₂ photocatalyst with visible light activity for NO removal. *J. Mol. Catal. A-Chem.* **161**, 205–212 (2010).
- Fujiwara, K. & Sotiris, E. P. Single Pd atoms on TiO₂ dominate photocatalytic NO_x removal. *Appl. Catal. B-Environ.* **226**, 127–134 (2018).
- Ma, J., Wang, C. & He, H. Enhanced photocatalytic oxidation of NO over g-C₃N₄-TiO₂ under UV and visible light. *Appl. Catal. B-Environ.* **184**, 28–34 (2016).
- Huang, C. et al. Visible light photocatalytic degradation of nitric oxides on PtO_x-modified TiO₂ via sol-gel and impregnation method. *J. Mol. Catal. A-Chem.* **316**, 163–170 (2010).
- Martins, N. C. T. et al. N-doped carbon quantum dots/TiO₂ composite with improved photocatalytic activity. *Appl. Catal. B-Environ.* **193**, 67–74 (2016).
- Baghbanzadeh, M., Carbone, L., Cozzoli, P. D. & Kappe, C. O. Microwave-assisted synthesis of colloidal inorganic nanocrystals. *Angew. Chem. Int. Ed.* **50**, 11312–11359 (2011).
- Kappe, C. O., Pieber, B. & Dallinger, D. Microwave effects in organic synthesis: myth or reality? *Angew. Chem. Int. Ed.* **52**, 1088–1094 (2013).
- Saib, A. et al. Carbon nanotube composites for broadband microwave absorbing materials. *IEEE T. Microw. Theory* **54**, 2745–2754 (2006).
- Menéndez, J. et al. Microwave heating processes involving carbon materials. *Fuel Process. Technol.* **91**, 1–8 (2010).
- Hu, X. & Yu, J. C. Continuous Aspect-Ratio tuning and fine shape control of monodisperse alpha-Fe₂O₃ nanocrystals by a programmed microwave-hydrothermal method. *Adv. Funct. Mater.* **18**, 880–887 (2008).
- Hu, X., Yu, J. C., Gong, J., Li, Q. & Li, G. alpha-Fe₂O₃ nanorings prepared by a microwave-assisted hydrothermal process and their sensing properties. *Adv. Mater.* **19**, 2324–2329 (2007).
- Zhang, L. & Zhu, H. Dielectric, magnetic, and microwave absorbing properties of multi-walled carbon nanotubes filled with Sm₂O₃ nanoparticles. *Mater. Lett.* **63**, 272–274 (2009).
- Zhang, D. et al. Microwave-antenna induced in situ synthesis of Cu nanowire threaded ZIF-8 with enhanced catalytic activity in H₂ production. *Nanoscale* **8**, 7749–7754 (2016).
- Grant, E. & Halstead, B. J. Dielectric parameters relevant to microwave dielectric heating. *Chem. Soc. Rev.* **27**, 213–224 (1998).
- Ye, Z., Deering, W. D., Krokhn, A. & Roberts, J. A. Microwave absorption by an array of carbon nanotubes: a phenomenological model. *Phys. Rev. B* **74**, 075425 (2006).
- Kane, C. L. & Mele, E. Size, shape, and low energy electronic structure of carbon nanotubes. *Phys. Rev. Lett.* **78**, 1932 (1997).

Acknowledgements

This work was supported by NSFC (21237003, 21261140333, 21477079, 21207090, 21876112, 21876113, 21761142011, NRF2017NRF-NSFC001-007), China Postdoctoral Science Foundation (2018M630981), Shanghai Government (18SG41, S30406, 13YZ054, 14ZR1430900, 18JC1412900, 18DZ2254200), PCSIRT (IRT1269).

Author contributions

D.Z. and H.L. conceived and designed the experiments. S.X., D.P., W.Z. and Y.C. performed the experiments. S.X. and P.L. analyzed the data. S.X. and G.L. wrote the manuscript. All authors discussed the results and commented on the manuscript.

Additional information

Supplementary Information accompanies this paper at <https://doi.org/10.1038/s41467-019-09509-y>.

Competing interests: The authors declare no competing interests.

Reprints and permission information is available online at <http://npg.nature.com/reprintsandpermissions/>

Journal peer review information: *Nature Communications* thanks Tao Zhang, Yongfa Zhu and the other anonymous reviewer(s) for their contribution to the peer review of this work.

Publisher's note: Springer Nature remains neutral with regard to jurisdictional claims in published maps and institutional affiliations.



Open Access This article is licensed under a Creative Commons Attribution 4.0 International License, which permits use, sharing, adaptation, distribution and reproduction in any medium or format, as long as you give appropriate credit to the original author(s) and the source, provide a link to the Creative Commons license, and indicate if changes were made. The images or other third party material in this article are included in the article's Creative Commons license, unless indicated otherwise in a credit line to the material. If material is not included in the article's Creative Commons license and your intended use is not permitted by statutory regulation or exceeds the permitted use, you will need to obtain permission directly from the copyright holder. To view a copy of this license, visit <http://creativecommons.org/licenses/by/4.0/>.

© The Author(s) 2019